Optics Letters

Spectral purity improvement of high-power pulsed lasers achieved by manipulating the nonlinear optical frequency conversion

Yanlin Zhang,[1,†] Pixian Jin,[1,2,†] Jie Yang,[1] Xiaojun Jia,[1,2] Huadong Lu,[1,2,3,*] and Kunchi Peng[1,2]

[1]State Key Laboratory of Quantum Optics Technologies and Devices, Institute of Opto-Electronics, Shanxi University, Taiyuan 030006, China
[2]Collaborative Innovation Center of Extreme Optics, Shanxi University, Taiyuan 030006, China
[3]National Key Laboratory of Particle Transport and Separation Technology, Tianjin, China
[†]These authors contributed equally to this work.
*luhuadong@sxu.edu.cn

Received 27 February 2025; revised 20 April 2025; accepted 30 April 2025; posted 30 April 2025; published 9 May 2025

Pulsed lasers usually suffer from the conflict between low spectral purity (SP) and high output power because the mode-selection process is not able to be accomplished within a short pulse period. In order to address this issue, we present a fresh lossless mode-selection method (MSM) that is implemented by manipulating the loss induced by nonlinear optical frequency conversion (LINOFC). Based on this method, the SP up to 3.2×10^4 with 9.16 W output power is experimentally obtained, which is attributed to the stronger and faster process of nonlinear optical frequency conversion (NOFC). In the experiment, in order to manipulate the magnitude of LINOFC during the short pulse period, a fast polarization control module based on an electro-optic effect was designed to change the phase-matching condition of fundamental light in the nonlinear crystal. Differing from the traditional MSMs, the NOFC will be more effective when the output power is increased; thus, a higher SP and a large output power can be achieved simultaneously in pulsed lasers, which is a type of necessary source for quantum optics and photonics technologies. © 2025 Optica Publishing Group. All rights, including for text and data mining (TDM), Artificial Intelligence (AI) training, and similar technologies, are reserved.

https://doi.org/10.1364/OL.560765

All-solid-state single-frequency pulsed lasers (SFPL) have been broadly applied in lots of fields including LiDAR, optical communication, high-precision spectral measurement, gravitational-wave detection, and so on, owing to their intrinsic advantages of narrow linewidth, low noise, and high coherence [1–3]. However, it is well-known that a pulsed laser usually works with a multi-longitudinal-mode operation at the beginning of pulse building-up because its gain is much higher than the loss then. Although the photon proportion of the dominant mode will continuously increase with the pulse building-up, it is still difficult to achieve a SFPL if the round trip times within a pulse period and the mode-loss difference are not enough to suppress the oscillation of sub-longitudinal-modes (SLMs) [4]. To address this issue, some mode-selection elements, such as etalons, are initially employed to introduce the mode-loss difference for the SLM suppression [5]. In 2020, Jin *et al.* realized a single-longitudinal-mode Pr:YLF laser with a pulse energy of 3.94 μJ and a pulse width of 81.1 ns at a repetition rate of 10 kHz using the Q switching pre-lase technology combined with the etalon. However, the output power is only 39.4 mW due to the large insertion loss [6]. Another method to obtain a SFPL is introducing a nonlinear mechanism to an oscillator, such as a passive Q-switched laser including a saturable absorber (SA). In 2005, Pan *et al.* achieved a single-longitudinal-mode Nd:$GdVO_4$ laser with a semiconductor saturable absorption mirror as the SA. The maximal average output power is 1.24 W at a repetition rate of 76.3 kHz, and the pulse width is 150 ns [7]. The SA can extend the round trip times and then make sure the laser works with a single-frequency operation. Nevertheless, with the increase of output power, the doped particles in the SA will be easily bleached in a very short time, which directly decrease the round trip times and thus further break the single-frequency operation condition. For reducing the influence of the bleaching effect, the doping concentration of the SA should be increased, which increases the absorption loss of the laser. Moreover, a short laser cavity has to be applied for achieving the good single-frequency output performance, which will also restrict the output power [8,9]. Compared to the above presentations, the single-frequency seed-injection locking is the most popular candidate for attaining the high-power SFPL [10,11]. In 2019, Cao *et al.* demonstrated an injection-seeded Q-switched Nd:YVO_4 ring laser with a pulse energy of 1.5 mJ and a pulse width of 8.1 ns at a repetition rate of 5 kHz, corresponding to an output power of 7.5 W. However, the adopted single-frequency seed laser and feedback control loop for stable single-longitudinal-mode operation will make the overall SFPL system complex and enormous [12]. In a word, it is difficult to realize a compact high-power nanosecond SFPL with high spectral purity based on the methods previously reported.

In this Letter, we propose a novel method to obtain a compact high-power SFPL with high spectral purity, which is achieved with the assistance of the intra-cavity loss induced by nonlinear optical frequency conversion (LINOFC). LINOFC increases the loss difference between the dominant mode and SLMs at the

beginning of the pulse building-up because of the sum-frequency process of different-mode radiations. At the same time, unlike the traditional methods of mode-selection, benefiting from the responding-time-free of nonlinear optical ferquency conversion (NOFC), the number of the SLMs is much lower than that of past systems at the beginning of the pulse building-up. Moreover, with the building-up of the laser pulse, the net gain proportion between the dominant mode and SLMs becomes higher and higher; thus, the number of the SLMs must further decrease quickly and a stable SFPL is attained lastly. The presented calculations and experimental results indicate that with the assistance of LINOFC, the SLMs are rapidly annihilated within a few nanoseconds, and a high-power SFPL with high spectral purity is achieved.

When LINOFC is introduced to the resonator, the loss factor δ is revised as [13]

$$\delta' = \delta + l_{\mathrm{NL}}, \tag{1}$$

where the nonlinear loss l_{NL} is equal to [13,14]

$$l_{\mathrm{NL}}(\nu_j) = kI(\nu_j) + 2k\sum_{i\neq j} I(\nu_i). \tag{2}$$

In Eq. (2), k represents the coupling strength between the nonlinear crystal and the fundamental laser, $I(\nu_j) = c\phi(\nu_j)h\nu$. When Eqs. (1) and (2) are substituted into the rate equation of multimode oscillation [15] and the spontaneous emission rate S that is added to the laser emission is also considered as the initial source of stimulated radiation [13], the dynamic process of the actively Q-switched laser may be theoretically simulated through the fourth-order Runge–Kutta method [15]. It is reasonable to consider that two adjacent modes α=ν_0 (ν_0 is the frequency corresponding to the peak value of gain profile) and β=ν_0+c/l (c and l are the speed of light in vacuum and the round trip cavity length, respectively) are simultaneously oscillating in the resonator, and μ=ϕ_α/ϕ_β is termed to the photon ratio of those two modes. When the gain crystal is supposed to be pumped with a peak pump power of 150 W, a duration of 75 μs, and a pump radius of 0.8 mm, the obtained inversion population density n is shown in Fig. 1(a_1), where the Nd:YVO_4 crystal is acted as the gain crystal and the round trip cavity length adopted for calculation is 830 mm. It is clear that when LINOFC is introduced into the resonator, the NOFC will effectively delay the decreasing speed of the inversion population density n. Moreover, owing to the effective coupling between LINOFC and the generated fundamental laser, the variation of the photon densities distributed over those two modes α and β is completely different, which is depicted in Figs. 1(a_2) and 1(a_3). The variation trends for both ϕ_α and ϕ_β are divided into four stages. In stage I, at the beginning of pulse building-up, the LINOFC is so weak that two modes will oscillate together. Although the building-up trends of adjacent dominant mode α and sub-mode β are almost the same, the small difference will be gradually amplified with the assistance of the LINOFC because of their sum-frequency effect through the nonlinear crystal [14]. As shown in stage II, the NOFC can decrease both ϕ_α and ϕ_β from P_{11} to P_{12} and from P_{21} to P_{22}, respectively, but ϕ_α descends more slowly than ϕ_β, and the difference between ϕ_α and ϕ_β is gradually enlarged. In this case, the mode α will gradually consume the gain of the mode β through the mode competition process. As a result, ϕ_β quickly decreases to the spontaneous radiation level from P_{22} to P_{23}, as shown in stage III. At last, ϕ_α is much greater than ϕ_β and μ reaches the peak value of 3.5×10^4 (P_4); as illustrated in stage IV, a SFPL with high spectral purity is attained.

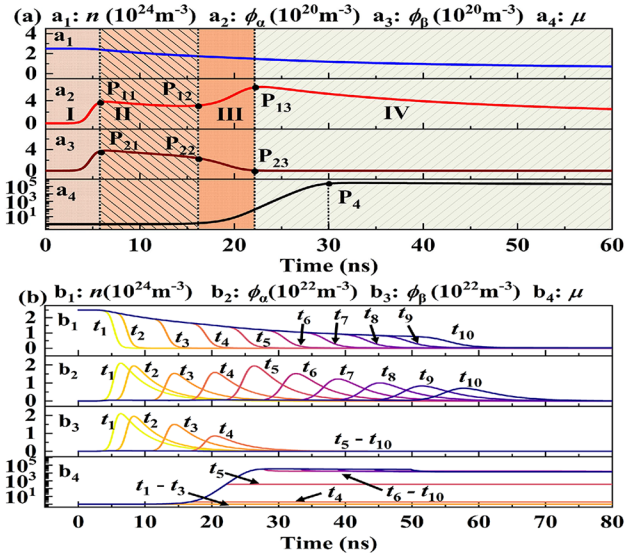

Fig. 1. (a) Dynamic of the actively Q-switched laser with nonlinear coupling strength k=1×10^{-10} m^2/W. (b) Dynamics under different t_k, t_1, 0ns; t_2, $2t_r$; t_3, $4t_r$; t_4, $6t_r$; t_5, $8t_r$; t_6, $10t_r$; t_7, $12t_r$; t_8, $14t_r$; t_9, $16t_r$; and t_{10}, $18t_r$.

Although the SFPL can be realized based on LINOFC, ϕ_α is far smaller than n, and the fall-time of the achieved pulse is too long, which must reduce its peak power. To address this issue, it is expected to remove the LINOFC as soon as possible once the SLMs are suppressed. Figure 1(b) depicts the variation trends of n, ϕ_α, ϕ_β, and μ during the pulse formation for different holding times of LINOFC (LINOFC is removed when the abscissa value is larger than the holding time), where the holding time t_k is normalized to the round trip time t_r. It is clear that μ is basically equal to 1 when the t_k is shorter than $4t_r$. When t_k is extended from $4t_r$ to $10t_r$, μ quickly increases from 1 to 3.5×10^4 because ϕ_α and ϕ_β quickly increase and decrease with the assistance of LINOFC, respectively. When t_k is further extended over $10t_r$, μ will not increase because ϕ_β has been decreased to the spontaneous emission level. Therefore, a SFPL with a narrow pulse width and high peak power will be obtained, while the LINOFC has be removed after $10t_r$.

To verify the proposed idea, we build up a butterfly shaped ring resonator depicted in Fig. 2. A composite a-cut YVO_4/Nd:YVO_4 crystal with a size of $3\times3\times(3+20)$ mm^3 (doping length: 20 mm) and a doping concentration of 0.8 at.% is employed as the gain medium, and it is pumped by a 888 nm laser diode (LD) with a maximum output power of 150 W. The optical isolator composed of a $\lambda/2$ wave plate (HWP) and Faraday rotator (FR) and acousto-optic Q-switch are inserted into the oscillator for unidirectional operation and pulsed laser generation, respectively. An output coupler with adjustable transmittance (OCAT) is well-designed, which consists of a $\lambda/2$ wave plate (HWP) and a polarization beam splitting (PBS1).

For introducing the LINOFC and manipulating the holding time t_k in the experiment, a fast LINOFC control module consisting of a nonlinear crystal and two electro-optic modulators (EOMs, EO1 and EO2) is ingeniously designed. A type-II phase-matched BBO with a size of $3\times3\times20$ mm^3 is chosen as the

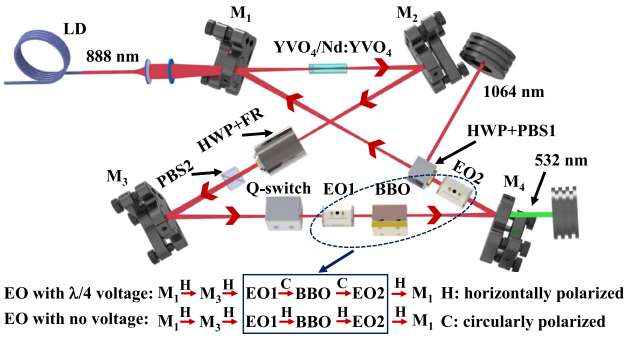

Fig. 2. Schematic diagram of the experimental setup for manipulating holding time t_k.

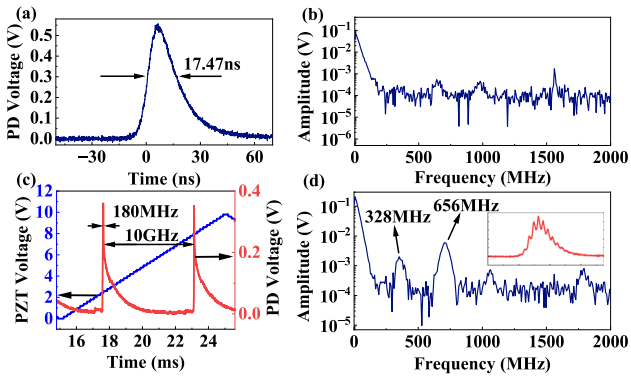

Fig. 3. Pulse waveform of 1064 nm laser (a); spectrum of the pulse waveform without BFS obtained by the Fourier transform (b); transmission signal of the scanned F–P cavity (c); and spectrum of the pulse waveform with BFS obtained by the Fourier transform (d).

nonlinear crystal to introduce LINOFC owing to its higher effective nonlinear coefficient. EO1(EO2) acts as a $\lambda/4$ wave plate on which a high-voltage signal with $\lambda/4$-voltage is applied. The laser polarization evolution is shown in Fig. 2. Since the electrodes of EO1 and EO2 are opposite in the design, when the propagation direction of the oscillating laser in the resonator is M_1-M_2-M_3-M_4-M_1, the horizontal polarized oscillating laser will become the circularly polarized laser after it passes through the $\lambda/4$-voltage supplied EO1. Then, the fractional oscillating laser will be converted to the second-harmonic laser in the BBO crystal, and the LINOFC is introduced. The residual circularly polarized oscillating laser changes back to the horizontal polarized laser again when it is passed through the $\lambda/4$-voltage supplied EO2. However, once the high-voltage signals are removed from EO1 and EO2, the polarization state of the oscillating laser will not be changed, and the oscillating laser is not converted to the second-harmonic laser, so the LINOFC is eliminated. Benefiting from the fast response of the EOM, the response time of the LINOFC manipulation is less than several nanoseconds, which is shorter than the pulse width of high-power Q-switched lasers (always tens of nanoseconds).

When the pump laser is driven by a pulsed power supply with a duration of 75 μs at the pulse repetition rate (PRR) of 4 kHz and the incident angle of the fundamental wave on the BBO crystal is optimized for its optimal phase matching, a single-frequency pulsed 1064 nm laser with an average output power of 5 W and a pulse width of 17.47 ns is obtained when the high-voltage signals are supplied on both EO1 and EO2. The second-harmonic 532 nm laser is obtained simultaneously with an average power and a pulse width of 1.7 W and 11 ns, respectively. The measured beam radius of 1064 nm in the gain crystal and the nonlinear crystal are 800 μm and 125 μm, respectively. According to the above experimental results, $k = 9.92 \times 10^{-11}$ m^2/W is calculated [13], which is close to the value utilized in our theoretical analysis. The pulse waveform is smooth without beat frequency signal (BFS), as shown in Fig. 3(a), in which a single-frequency output is indicated [4,16]. To further ensure its single-frequency operation, a scanned F–P cavity is used for measuring the linewidth of the laser, as shown in Fig. 3(c). The linewidth determined by the full width at half maximum (FWHM) of the transmission signal of the scanned F–P cavity is measured to be 180 MHz. The linewidth is narrower than the free spectral region (FSR) of the resonator of 328 MHz (the equivalent optical length of the resonator is 910 mm), further indicating that the obtained 1064 laser works with a single-longitudinal-mode operation. On the contrary, when the high-voltage signals supplied to EO1 and EO2 are removed, the pulsed 1064 nm laser with an average power of 10.32 W is obtained, and its pulse waveform has a clear BFS with frequencies of 328 MHz and 656 MHz obtained by the Fourier transform, which is consistent with the FSR of the resonator, as shown in Fig. 3(d). This indicates that the BFS in the pulse waveform is formed due to the beat nodes between different longitudinal oscillating modes in the resonator. The values of μ is measured by means of the BFS amplitude of adjacent longitudinal modes in the Fourier transform spectrum. The BFS amplitude between modes α and β in the pulse waveform is written as [17]

$$I_M = \kappa E_\alpha E_\beta \cos(2\pi ct/L), \tag{3}$$

where κ is a constant representing a scale factor. Usually, the number of photons in the mode α is significantly greater than that in the mode β; thus, the DC part of the pulse waveform is represented as $I_D = \kappa E_\alpha^2/2$. In this case, we have

$$\mu = \left[\frac{2I_D \cos(2\pi ct/L)}{I_M}\right]^2. \tag{4}$$

Especially, $\cos(2\pi ct/L) = 1$ corresponds to the peak of BFS in the pulse waveform and then $\mu = 4(I_d/I_M)^2$. In this case, the value of μ will be obtained directly from the pulse waveform. For the pulse waveform given in Fig. 3(d), the amplitude of the BFS part is 78.1 mV, the voltage of the DC part is 381.8 mV at the peak point, and the corresponding μ of 95.6 is calculated, while the corresponding μ of 1.41×10^4 is obtained for the pulse waveform in Fig. 3(a).

The above experimental results showed that the LINOFC can suppress the SLMs during the pulse building process, and thus a stable SFPL will be obtained. However, the mode-selection loss introduced by the LINOFC is about 50% in the presented experiment. According to the theoretical expectation, the mode-selection loss may be further reduced by manipulating the holding time t_k, and then a high-power SFPL can be obtained. In the experiment, t_k is manipulated by adjusting the delay between the rising edge of the laser pulse and the falling edge of the high-voltage signal (DPHV), and the obtained pulse waveforms at different DPHVs are shown in Fig. 4(a). The corresponding amplitudes of BFSs obtained by FFT are shown in Fig. 4(b). It is obvious that the BFS in the pulse waveform gradually disappears with the increase of DPHV, and the amplitude of the BFS

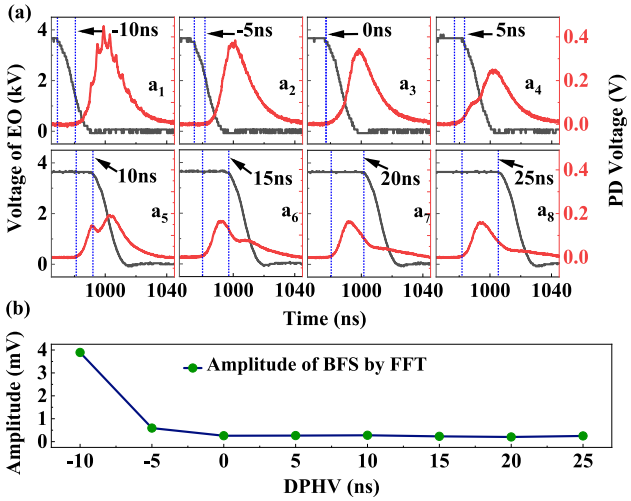

Fig. 4. Pulse waveforms (a) and the amplitudes of BFS by FFT (b) under different DPHVs.

reaches a relatively stable low level when the DPHV is larger than 0 ns owing to the limited resolution of the utilized oscilloscope in the experiment. The obtained values of μ and average output powers at different DPHVs are shown in Fig. 5. With the DPHV increasing from −10 ns to 0 ns, the value of μ grows rapidly from 161.5 to 3.2×10^4, but an output power of 1064 nm only decreases from 10.32 W to 9.16 W. So, the mode-selection loss introduced by LINOFC is only 11.2%. According to the theoretical calculation, the value of μ should be the same as or higher than that at DPHV of 0 ns when the DPHV is increased larger than 0 ns. However, the value obtained in the experiment decreases gradually to about 1.0×10^4. This may be resulted from the limited resolution of the oscilloscope, which is also a probably reasonable consideration for why the highest value of μ realized in the experiment is much smaller than that calculated from the theoretical formula. The results demonstrate that a high-power SFPL with high spectral purity (up to 3.2×10^4) and small mode-selection loss (11.2%) may be obtained by adjusting the DPHV. Furthermore, the falling edge of the high-voltage signal supplied to the EOM is about 20 ns, which is close to the pulse width of the laser, so the overdamped NOFC cannot be suppressed as fast as required, which will introduce an extra mode-selection loss. If the falling edge of the high voltage is further shortened and the measurement resolution of the BFS is further enhanced, the high-power SFPL with a higher spectral purity and less mode-selection loss will be possibly achieved.

In conclusion, we presented a novel scheme for improving the spectral purity of pulsed lasers based on the LINOFC and experimentally verify the feasibility of this method. The spectral purity of dominant mode is able to reach four orders of magnitude, which is totally different from that obtained with traditional SFPL methods and overcomes the bargain between high output power and high spectral purity. By adjusting the DPHV to change the holding time t_k, the suppression effect of LINOFC on the SLMs is further verified experimentally. Compared with traditional methods, this method not only achieves much higher spectral purity at a stably higher output power but also has advantages of miniaturization, and compactness, which plays a crucial

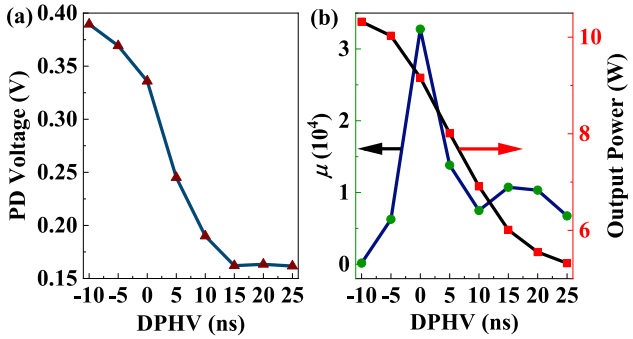

Fig. 5. Variation of the PD detector voltage of DC (a), μ and output power of 1064 nm (b) versus DPHV.

role in popularizing SFPL. The achieved good results revealed that it is easy to obtain the different wavelength pulsed lasers with high power and high spectral purity only if the gain and nonlinear media were replaced. Moreover, the presented method is beneficial to obtain a pulsed laser with higher output power by removing the nonlinear loss once the single-longitudinal-mode operation of the pulsed laser is built. At the same time, the pulse width of the laser can also be narrowed. Therefore, the high-power SFPL with high spectral purity presented in this Letter may promote the further development of optical information fields such as quantum precision measurement, LiDAR, and optical sensors.

Funding. National Key Research and Development Program of China (2022YFC2204003); Shanxi Scholarship Council of China (2022-015); Science and Technology Innovation Group of Shanxi Province (20220405100200 5); The First Lab - National Innovation Center (Shanxi) Science and Technology Innovation Project; National Key Laboratory of Particle Transport and Separation Technology (KWKF-2024-2).

Disclosures. The authors declare no conflicts of interest.

Data availability. Data underlying the results presented in this Letter are not publicly available at this time but may be obtained from the authors upon reasonable request.

REFERENCES

1. S. Luo, Z. Cai, H. Xu, *et al.*, Opt. Laser Technol. **116**, 112 (2019).
2. B.-Q. Yao, X.-M. Duan, D. Fang, *et al.*, Opt. Lett. **33**, 2161 (2008).
3. H. Zhang, M. Long, H. Deng, *et al.*, Chin. Opt. Lett. **17**, 44 (2019).
4. A. E. Siegman, *Lasers* (University Science Books, 1986).
5. A. Berry, D. Hanna, and C. Sawyers, Opt. Commun. **40**, 54 (1981).
6. L. Jin, W. Dai, Y. Yu, *et al.*, Opt. Laser Technol. **129**, 106294 (2020).
7. H. Pan, S. Xu, and H. Zeng, Opt. Express **13**, 2755 (2005).
8. W. Sooy, Appl. Phys. Lett. **7**, 36 (1965).
9. D. Jones and D. Rockwell, Appl. Opt. **32**, 1547 (1993).
10. J. Zhang, X. Zhu, H. Zang, *et al.*, Appl. Opt. **53**, 7241 (2014).
11. C. Chen, C. Gao, H. Dai, *et al.*, Chin. Opt. Lett. **20**, 041402 (2022).
12. X. Cao, P. Li, and Q. Liu, Appl. Opt. **58**, 8565 (2019).
13. W. Koechner, *Solid-State Laser Engineering* (Springer, 2006).
14. K. Martin, W. Clarkson, and D. Hanna, Opt. Lett. **22**, 375 (1997).
15. Y. Li, W. Tu, B. Wang, *et al.*, IEEE Photonics J. **10**, 1 (2018).
16. G. J. Koch, M. Petros, J. Yu, *et al.*, Appl. Opt. **41**, 1718 (2002).
17. X. Wang, S. Wang, Z. Zhou, *et al.*, Appl. Opt. **62**, 6672 (2023).